CrystEngComm

PAPER

View Article Online
View Journal | View Issue

Check for updates

Cite this: *CrystEngComm*, 2023, **25**, 3790

Substituent effects on the [1-*closo*-CB_9H_{10}]$^-$ anion geometry: experimental and DFT studies†

Anna Pietrzak, *[a] Michael J. Carr[b] and Piotr Kaszyński *[cde]

Received 12th April 2023,
Accepted 6th June 2023

DOI: 10.1039/d3ce00357d

rsc.li/crystengcomm

Five new structures of the [*closo*-1-CB_9H_{10}]$^-$ anion substituted at the apical position(s) are reported expanding the pool of such derivatives to a total of 35. Geometrical features of twenty four of these experimental structures are compared to those obtained by full geometry optimization at the B3LYP/Def2TZVP level of theory. The range of derivatives permitted analysis of the substituent effect on the {*closo*-1-CB_9} cluster geometry as a function of Hammett parameters σ_p, which revealed a substantial impact of the B(10) substituent and negligible effect of the C(1) group. This structural report and analysis are accompanied by an overview of the progress in the development of functional derivatives of the [*closo*-1-CB_9H_{10}]$^-$ anion and methods of their preparation.

Open Access Article. Published on 07 June 2023. Downloaded on 12/18/2025 6:25:32 PM.
This article is licensed under a Creative Commons Attribution-NonCommercial 3.0 Unported Licence.

Introduction

Carbaborate anions[1] [*closo*-1-$CB_{11}H_{12}$]$^-$ and [*closo*-1-CB_9H_{10}]$^-$ (**1a**, Fig. 1) are of increasing importance as structural elements of functional materials,[2,3] such as ionic liquids,[4–6] ionic liquid crystals,[7–9] electrolytes[10–12] for energy storage, and polar liquid crystals[13–16] investigated for display applications. Many of these applications require substitution patterns in antipodal positions, 1 and 12 for the former anion, and 1 and 10 in **1a**, to obtain structures with elongated molecular shapes. Therefore there is significant interest in synthetic and structural chemistry of both clusters with such substitution patterns. While substantial effort has been directed to the larger cluster, [*closo*-1-$CB_{11}H_{12}$]$^-$, the smaller, 10-vertex anion **1a** receives much less attention. This is evident from *e.g.*, the number of single crystal structures deposited in Cambridge Structural Database (CSD). Thus, there is a total of 740 structures containing the {*closo*-1-CB_{11}} cluster and 301 with substitution at the antipodal positions. In contrast, there are only 88 reported structures with the {*closo*-1-CB_9} skeleton (62 with organic substituents and 26 with organometallic groups), out of which only 30 have substituents at the C(1), B(10) or both positions.

The disproportionally low number of {*closo*-1-CB_9} structures with apical substituents deposited in CSD is related to the fact that convenient access to the parent 10-vertex anion **1a** was developed relatively late, about two decades ago.[17,18] Prior to 2000 structure of the parent **1a** (ref. 19) and its 8 derivatives were reported, out of which only one, the C(1)–NMe_3 derivative **1b**,[20] had an apical substituent.

The new three-step Brellochs' method,[17] involving thermal rearrangement of the {*closo*-2-CB_9} intermediates, opened up a relatively efficient access to the parent anion [*closo*-1-CB_9H_{10}]$^-$ (**1a**)[11] and its C(1) substituted derivatives (Fig. 2). Consequently, several compounds were obtained directly, such as **1c**,[21,22] **1d**,[23] **1e**,[18] **1f**,[24] **1g**,[25] **1h**,[24] or through simple chemical transformations (**1i**,[26] **1j**,[27] and **1k** (ref. 24)) and their structures were reported (Fig. 1). Other derivatives, such

Y = H
a, X = H
b, X = NMe_3^+
c, X = Ph
d, X = C_6H_4-4-F
e, X = C_6H_4-4-Br
f, X = C_6H_4-4-COOH
g, X = C_6H_4-4-CN
h, X = COOH
i, X = C_6H_4-4-N_2^+
j, X = CONHPr-*i*
k, X = CH_2OH
l, X = Cl
m, X = N=NC_6H_4-4-NH_2
n, X = SMe_2^+
o, X = 2-$C_5H_5N^+$

Y = I
p, X = Ph
q, X = N_2^+
v, X = $CH_2CH_2C_6H_4$-4-OMe

X = COOH
r, Y = N_2^+
s, Y = 1-$C_5H_5N^+$
t, Y = 1-$(CH_2)_5S^+$

Y = PhI$^+$
u, X = $CH_2CH_2C_6H_4$-4-OMe

X = H
w, Y = N_2^+
x, Y = 1-$C_5H_5N^+$
y, Y = MeC(=NH_2)NH^+

Fig. 1 Structures of derivatives **1**. Each vertex represents a BH or B (when substituted) fragment and the sphere is a carbon atom.

[a] *Faculty of Chemistry, Łódź University of Technology, 90-924 Łódź, Poland. E-mail: anna.pietrzak.1@p.lodz.pl*
[b] *School of Chemistry of the University of Leeds, Leeds, England, UK LS2 9JT, UK*
[c] *Faculty of Chemistry, University of Łódź, 91-403 Łódź, Poland*
[d] *Centre of Molecular and Macromolecular Studies, Polish Academy of Sciences, 90-363 Łódź, Poland*
[e] *Department of Chemistry, Middle Tennessee State University, Murfreesboro, TN, 37130, USA*

† Electronic supplementary information (ESI) available: XRD data collection and refinement, details of CSD search, experimental and DFT structural data, additional correlation plots, and DFT computational results. CCDC 265347–265351. For ESI and crystallographic data in CIF or other electronic format see DOI: https://doi.org/10.1039/d3ce00357d

This journal is © The Royal Society of Chemistry 2023

Open Access Article. Published on 07 June 2023. Downloaded on 12/18/2025 6:25:32 PM.
This article is licensed under a Creative Commons Attribution-NonCommercial 3.0 Unported Licence.

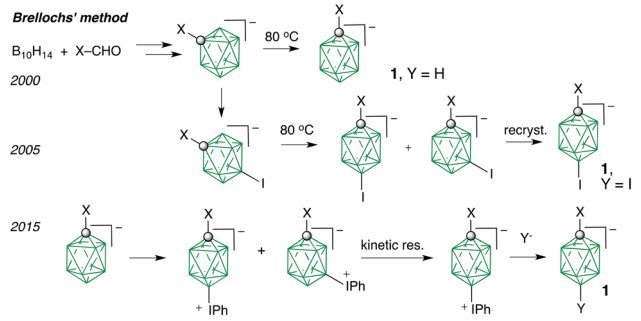

Fig. 2 Evolution of modern methods for the synthesis of apical-substituted derivatives of **1a**.

as **1l**, **1m**, **1n**, and **1o** were prepared[28] through chemical transformations of the COOH group in **1h**, but their XRD structures were not reported. Soon after the discovery of the Brellochs' method, it was demonstrated[29] that thermal rearrangement of easily obtainable 7-halo {*closo*-2-CB_9} derivatives lead to a mixture of 1,6- and 1,10-disubstituted derivatives of the [*closo*-1-CB_9H_{10}]$^-$ anion (Fig. 2), and the structure of the first 1,10-difunctionalized derivative **1p** was reported.[29] This discovery was exploited in 2005 in the development of a practical access to a broad range of 1,10-difunctionalized derivatives of **1a**, such as **1q**,[9] starting with the isomerically pure [*closo*-1-CB_9H_8–1-COOH-10–I]$^-$.[30]

Transformation of the iodo substituent led to the dinitrogen zwitterion **1r**, which was converted to pyridinium **1s** and sulfonium derivative **1t**.[31] Crystal structures of all three 1-carboxylic acid derivatives, **1r–1t**, were reported.[31]

A more efficient and general method for the preparation of B(10) substituted derivatives of the [*closo*-1-CB_9H_{10}]$^-$ anion was discovered in 2015 (Fig. 2).[32] Unlike the Brellochs' procedure, the new method relies on substitution of the parent **1a** and its C(1) derivatives with a phenyliodonium group, which undergoes a nucleophilic displacement or can be reduced to the iodo substituent. The proportion of the B(10) *vs.* B(6) substitution is about 1 : 1, the highest to date for an electrophilic substitution of **1a**, but the two regioisomers are conveniently resolved by differential reactivity with nucleophiles (kinetic resolution).[33] This method was used to obtain zwitterionic derivative **1u**, which was transformed to the B(10)–iodo derivative **1v**.[34] Analogous transformations of the parent **1a** led to B(10) derivatives **1w–1y**.[33] Crystal structures of all five derivatives have been established and reported.[33,34] This demonstrates a significant potential for further development of 1,10-difunctional derivatives of **1a**.

The growing number of derivatives brings up a question whether there is a pattern in response of the {*closo*-1-CB_9} skeleton geometry to the electronic nature of apical substituents. Such relationships were found in derivatives of the related dianion [*closo*-$B_{10}H_{10}$]$^{2-}$, in which the B(1)···B(10) separation decreases with an increasing electron-withdrawing character of the substituent(s).[35–37] This leads to a question, whether this trend is specific to the [*closo*-$B_{10}H_{10}$]$^{2-}$ dianion derivatives or more universal and applicable also to derivatives of the [*closo*-1-CB_9H_{10}]$^-$ anion (**1a**).

Herein we report structural data for 5 derivatives of the [*closo*-1-CB_9H_{10}]$^-$ anion substituted in the C(1) position (**1l**, **1m**, **1n**, and **1o**, Fig. 1) or C(1) and B(10) positions (**1q**). Geometry of these compounds together with that of 19 similar structures, selected from the crystallographic database and containing simple substituents with known electronic characteristics (Fig. 1), are analyzed in detail. The experimental structural parameters of the entire set of 24 compounds are compared to those obtained from DFT calculations. Finally, substituent effects on the {*closo*-1-CB_9} cluster geometry are analyzed using Hammett constants.

Experimental

X-ray crystallography

Single-crystal X-ray diffraction measurements for **1l[PyrCH$_2$-Cl]**, **1m[Et$_4$N]·[Et$_4$NBr]**, **1n**, **1o** and **1q** were performed with a Bruker Nonius Kappa CCD diffractometer. The crystals were kept at 150(2) K during data collection, while measurements for **1o** were conducted at 195(2) K. Data collections were performed using the Mo Kα radiation (λ = 0.71073 Å).[38,39] All structures were solved using direct methods by ShelXS-97 (ref. 40) and refined in the ShelXL-97.[41] All non-hydrogen atoms were refined anisotropically. C–H and B–H hydrogens were generated geometrically using the HFIX command in ShelXL. Additional data collection and refinement information is listed in ESI.†

CCDC files 265347–265351 contain the ESI† crystallographic data for new structures.

Computational details

Quantum-mechanical calculations were carried out using Gaussian 09 suite of programs. Geometry optimizations were undertaken using the B3LYP[42,43] functional with Karlsruhe triple-ζ polarization Def2TZVP basis set[44,45] and tight convergence limits with appropriate symmetry constraints. All calculations were performed in PhCl dielectric medium (arbitrarily chosen) with the PCM model[46] requested with SCRF(Solvent=C_6H_5Cl) keyword, since it was demonstrated[35] that low dielectric medium is important for obtaining accurate geometry of zwitterions. The ground state nature of stationary points for the obtained equilibrium geometry was confirmed with vibrational frequency calculations.

Results and discussion

Molecular and crystal structure

Crystals suitable for structural analysis were grown by slow evaporation of solutions of compounds reported previously:[9,28] **1l[PyrCH$_2$Cl]** (yellow prisms from CH_2Cl_2–Et_2O), **1m[Et$_4$N]·[Et$_4$NBr]** (yellow prisms from CH_3CN–Et_2O), **1n** (colorless prisms from CH_2Cl_2–*n*-hexane), **1o** (colorless needles from CH_2Cl_2–Et_2O), and **1q** (yellow crystals from CH_2Cl_2–*n*-hexane). Their solid-state structures were

Open Access Article. Published on 07 June 2023. Downloaded on 12/18/2025 6:25:32 PM.
This article is licensed under a Creative Commons Attribution-NonCommercial 3.0 Unported Licence.

determined by low temperature single crystal X-ray analysis, and the results are shown in Fig. 3–5. Full details of data collection, refinement and molecular geometry are provided in the ESI.†

Crystal structures of **1n**, **1o**, and **1q** are formed by single symmetry-independent molecules resulting in unit cells containing two molecules related by inversion (**1n**) or four molecules related by inversion and 2-fold rotoinversion axes (**1o** and **1q**, Fig. 3). In contrast, asymmetric units of **1l[PyrCH$_2$Cl]** and **1m[Et$_4$N]·[Et$_4$NBr]** contain two symmetry-independent pairs of ions. In addition, the asymmetric unit of the latter crystal contains two disordered ion pairs $[Et_4N]^+$ Br^-, which results in a cocrystal of **1m[Et$_4$N]** and **[Et$_4$NBr]**. Although both structures **1l[PyrCH$_2$Cl]** and **1m[Et$_4$N]·[Et$_4$NBr]** are characterized by $Z' = 2$, the respective symmetry independent ions adopt similar conformations, and their overlay gives low root-mean-square deviation (RMSD) values (*i.e.*, 0.007 for **1l[PyrCH$_2$Cl]** and 0.097 for **1m[Et$_4$N]·[Et$_4$NBr]**).

The two symmetry-independent anions **1l** are differentiated by their type of assembly within the crystal and nonbonding interactions with accompanying cations. The crystal system of **1l[PyrCH$_2$Cl]** is composed of chains formed by the anions linked through short contacts which are inside the van der Waals separation: −0.039 Å for Cl(1b)···B(10A) and −0.014 Å for B(7A)···H(9B). The chains are arranged parallel to the (010) planes separated by layers of 1-chloromethylpyridynium counterions (Fig. 4a). The crystal lattice stabilization is augmented by coulombic short contacts between the [*closo*-1-CB$_9$H$_9$–1-Cl]$^-$ anions and 1-chloromethylpyridinium cations.

Similarly to **1l[PyrCH$_2$Cl]**, crystal structures of **1n** and **1o** can be defined as layers formed by individual molecules (Fig. 4b and c). Supramolecular layers in zwitterion **1n** extend along the (110) plane. They are formed by S···B and C–H···B non-bonding interactions between the Me_2S^+ substituent and a B atom of the neighboring {*closo*-1-CB$_9$} cage and strengthen by B–H···B close contacts between adjacent molecules. The inter-layer contacts are provided through

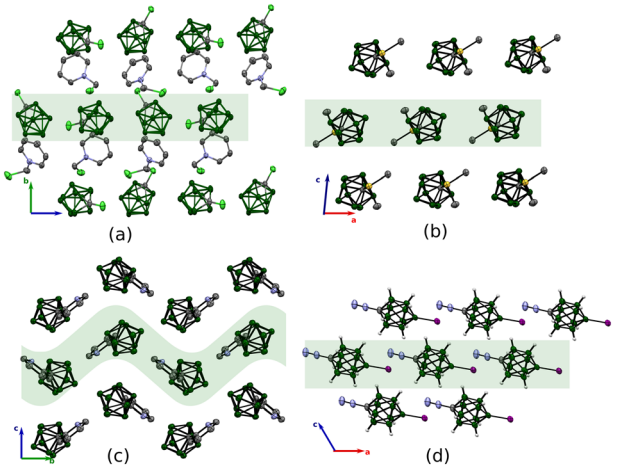

Fig. 4 Partial packing of **1l[PyrCH$_2$Cl]** (a), **1n** (b), **1o** (c) and **1q** (d). Hydrogen atoms and counterions are omitted for clarity.

C–H···B interactions between Me_2S^+ fragment and the {*closo*-1-CB$_9$} cage.

In the crystal structure of zwitterion **1o**, layers are parallel to the (110) plane and are stabilized by the N–H···B and C–H···B short contacts between the pyridine fragment and the {*closo*-1-CB$_9$} cage of the neighboring molecules, while contact between layers involves interactions of pyridine π-electron system and the {*closo*-1-CB$_9$} cage.

Molecules of **1q** form chains extending along the [100] direction (Fig. 4d) through B···I interactions between neighboring molecules. Adjacent chains are linked through B–H···B contacts between the {*closo*-1-CB$_9$} cages.

As in the structure of **1q**, supramolecular chains of **1m[Et$_4$N]·[Et$_4$NBr]** extend in the [100] direction. However, these infinite substructures are formed by [*closo*-1-CB$_9$H$_9$–1-(N=NC$_6$H$_4$–4-NH$_2$)]$^-$ and Br^- anions linked through interactions between the NH_2 groups and Br^- ions (Fig. 5). Neighboring chains in **1m[Et$_4$N]·[Et$_4$NBr]** are separated by

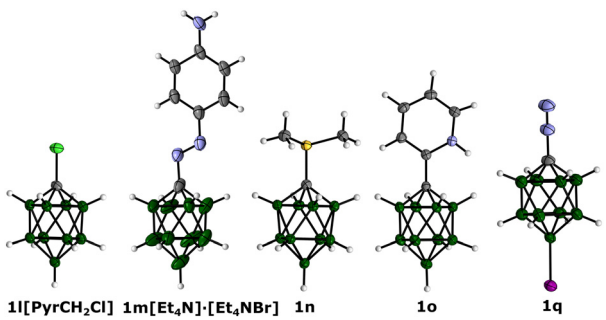

Fig. 3 Atomic displacement ellipsoid representation of **1l[PyrCH$_2$Cl]**, **1m[Et$_4$N]·[Et$_4$NBr]**, **1n**, **1o**, and **1q**. The atomic ellipsoids are set at the 50% probability level, and the numbering scheme is according to the chemical structures. For **1l[PyrCH$_2$Cl]** and **1m[Et$_4$N]·[Et$_4$NBr]** only one symmetry-independent molecule is shown, and accompanying ions are omitted for clarity. Full geometry parameters are listed in the ESI.†

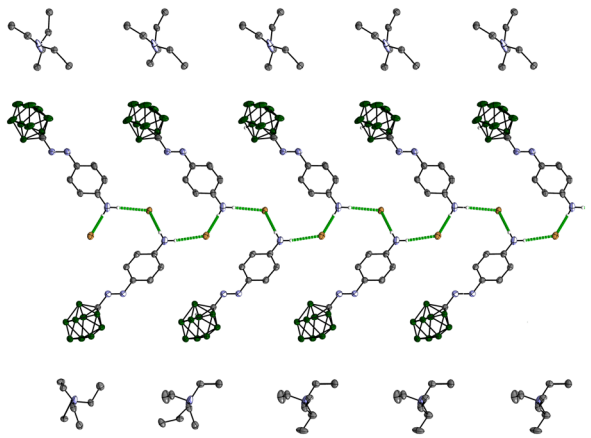

Fig. 5 Partial packing diagram for **1m[Et$_4$N]·[Et$_4$NBr]**. Hydrogen atoms not involved in the N–H···Br interactions are omitted. Only one disordered site of $[Et_4N]^+$ is shown for clarity.

This journal is © The Royal Society of Chemistry 2023

Open Access Article. Published on 07 June 2023. Downloaded on 12/18/2025 6:25:32 PM.
This article is licensed under a Creative Commons Attribution-NonCommercial 3.0 Unported Licence.

the $[Et_4N]^+$ counterions. Geometrical parameters of short contacts stabilizing the crystal systems are listed in the ESI.†

Cambridge structural database (CSD) search

For the purpose of a broader structural analysis, Cambridge Structural Database (CSD, version 5.43, November 2022) was searched to obtain a larger pool of experimental structural data using search criteria defined in Fig. 6.

The search yielded a total of 32 crystal structures containing the {*closo*-1-CB_9} skeleton with substituents at the C(1), B(10) or both apical positions and the parent **1a** (for the complete list see the ESI†). In the entire set, there are 29 structures with unique substitution on the {*closo*-1-CB_9} cluster and the parent, out of which 19 structures were selected as suitable for further investigation.

{*closo*-1-CB_9} cage geometry – a comparison of experimental and DFT results

In order to facilitate comparison of experimental and DFT-optimized structures, and also data analysis, geometrical parameters of the {*closo*-1-CB_9} skeleton were defined as shown in Fig. 7. The B(10)–B, B(6)–B(7), B(2)–B(6), B(2)–B(3), and B–C(1) distances are averaged and designated as d_{1B}, d_{2B}, s, d_{2C}, and d_{1C}, respectively. The *esd's* associated with these parameters reflect the distribution of individual values in both experimental and theoretical structures. Such an analysis of average parameters allows for avoiding conformational differences between the solid-state and DFT-derived geometries. DFT structures were obtained by full geometry optimization at the B3LYP/Def2TZVP level of theory in PhCl dielectric medium. This weak, arbitrary selected dielectric medium was demonstrated to be important for accurate geometry modeling.[35] All values used in the analysis are listed in the ESI.†

A comparison of all experimental and DFT-derived geometrical parameters defined in Fig. 7 for derivatives **1** shows an excellent correlation with $r^2 > 0.999$ and with the slope equal unity, and essentially no systematic error (Fig. 8). This demonstrates that in general the DFT method reproduces the experimental structures accurately. Detailed analysis of each group of parameters shows, however, some significant deviation from this general trend related mainly to the quality of some experimental data. Thus, analysis of the heights of the tetragonal pyramids demonstrates that h_B

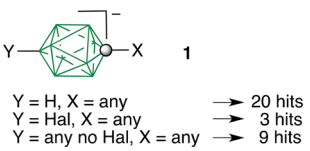

Fig. 6 Structural criteria used for the CSD search. Each vertex represents a BH or B (when substituted) fragment and the sphere is a carbon atom. Filters used: 3D coordinates determined, no errors, only single crystal structures, only organics.

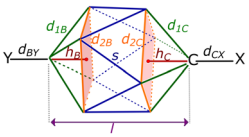

Fig. 7 Structural model of the {*closo*-1-CB_9} skeleton in derivatives **1** with defined geometrical parameters.

for the B(10) pyramid (Fig. 7) is more accurately reproduced by DFT (conforming to the general fitting line with $r^2 = 0.88$) and has a nearly 3 times larger span of values than the height of the C(1) pyramid (h_C, $r^2 = 0.75$, Fig. 9). Parameter h_B for **1q** (X = N_2^+, Y = I) exhibits the largest deviation (0.023 Å *vs.* the average of absolute differences of 0.005 Å) from the value expected on the basis of the general correlation (Fig. 8). Removing this data point improves correlation for h_B to $r^2 = 0.925$. The observed large deviation for **1q** is due, in part, to a relatively large error on individual bonds (*std* ~ 0.010 Å) and, in part, to difficulties with accurate modelling of the iodine atom with this DFT method.

The B–B distance s (Fig. 7) between the equatorial planes is nearly constant in the entire series and for most compounds is clustered within 0.015 Å. The only exceptions are **1d** (X=C_6H_4F) and **1q**, which differ from the DFT estimate by 0.032 and 0.015 Å, respectively, while the average value of the absolute differences in the series is about 0.006 Å and within a typical experimental error.[47] Inspection of the results indicates that the difference between the experimental and DFT values for the first derivative is related to large experimental errors, as evident from multiple B alerts in *Checkcif* validation procedure involving the Hirshfeld rigid bond test. In addition, molecules of **1d** exist as cocrystals with its 2-carba isomer, [*closo*-2-CB_9H_9–2-C_6H_4F]$^-$ in a 1 : 1 ratio from incomplete thermal rearrangement. In contrast, deviation for **1q** data point is presumably due to inaccurate DFT geometry modeling.

The total length l of the {*closo*-1-CB_9} cluster is a sum of tetragonal pyramid heights h and the separation between the

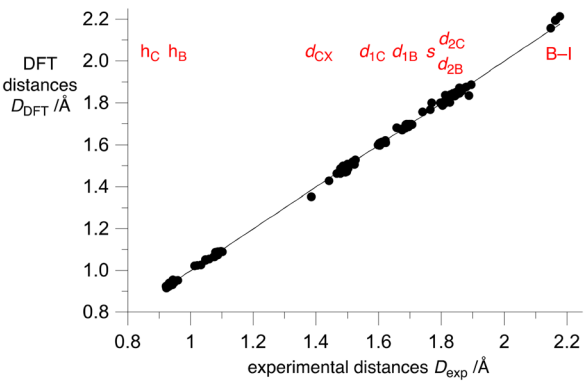

Fig. 8 A comparison of experimental and DFT-derived geometrical parameters D for the {*closo*-1-CB_9} cluster in series **1** defined in Fig. 7. Best fitting line $D_{DFT} = D_{exp} - 0.001(1)$, $r^2 = 0.999$. Numerical data are listed in the ESI.†

Open Access Article. Published on 07 June 2023. Downloaded on 12/18/2025 6:25:32 PM.
This article is licensed under a Creative Commons Attribution-NonCommercial 3.0 Unported Licence.

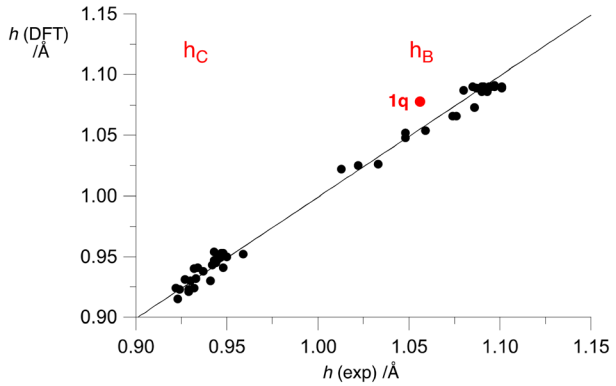

Fig. 9 A comparison of experimental and DFT-derived heights h of the tetragonal pyramid in the {*closo*-1-CB_9} cluster in series **1** defined in Fig. 7. The line is the overall best fitting line from Fig. 8. The red dot indicates the most outlying data point.

equatorial planes. A comparison of the experimental and DFT-calculated parameter l indicates good correlation with the exception of **1d** (*vide supra*). Without this data point the correlation is satisfactory (r^2 = 0.86).[47]

Other {*closo*-1-CB_9} cage dimensions include the length of the tetragonal pyramid edge d_1 and base d_2. The former parameter assumes values in two ranges: lower d_{1C} values are in a narrow range of 1.60–1.62 Å, while the d_{1B} values are between 1.65 and 1.71 Å (Fig. 10). These differences reflect the generally lower impact of the C(1) substituent on the cage geometry, when compared with the effect of the B(10) substitution.

All data points for the d_{1C} parameter appear close to the general fitting line, albeit due to a narrow range of the values the resulting correlation parameter is low (r^2 = 0.33). The largest differences from the expected values are observed for **1g** (X═C_6H_4CN, 0.07 Å) and again for **1d** (0.011 Å), while the distribution of the individual measurements is 0.005 and 0.020 Å. Removing these data points from the correlation improves r^2 to 0.55 and gives the average absolute difference between experimental and DFT values of 0.003 Å.

Similar analysis of the d_{1B} parameter demonstrates that the largest differences of about 0.01 Å are observed for **1j** (X═CONHPr-*i*), **1d** and **1q**, which are comparable with the *std* of the individual values constituting the averages. Removing these data points from the correlation increases r^2 value from 0.60 to 0.75. Inspection of structural data retrieved from Crystallographic Information File (CIF) for **1j** shows a relatively large R value of ~8% accompanied by elongated ellipsoids and a low precision of determining individual bonds of about 0.006 Å. This certainly contributes to the observed differences in the correlation.

The distances between equatorial boron atoms fall into a range essentially the same for both equatorial belts. As previously observed, values d_{2C} and d_{2B} for **1d** are far from the expected correlation with the largest deviations up to 0.050 Å for the former parameter (Fig. 11). Much smaller, nevertheless significant deviations are observed for **1j** (0.013 Å) and for **1q** (0.007 Å), while the average of absolute differences for the two parameters is 0.003 Å. Issues related to these three structures are described above.

Finally, analysis of exocyclic bonds at the apical positions of the [*closo*-1-CB_9H_{10}]$^-$ anion demonstrates a very good agreement between the experimental and DFT-derived distances d_{CX} and d_{BY} (Fig. 12). The largest differences are observed for the B–I bonds in derivatives **1p** (0.031 Å), **1r** (0.0315 Å), **1v** (0.035 Å), which are significantly larger than the experimental error of 0.006, 0.003 and 0.002 Å, respectively. At the same time, the mean difference between the remaining experimental and DFT *exo*-cage distances are 0.012 Å. This discrepancy indicates a systematic deficiency with accurate treatment of the iodine atom at this level of theory. Also the B–N bond in **1q** is calculated shorter, by 0.032 Å, than suggested by experiment, although this value has an associate large experimental error of ±0.020 Å.

The comparison of geometrical parameters indicates a generally high level of accuracy of the B3LYP/Def2TZVP

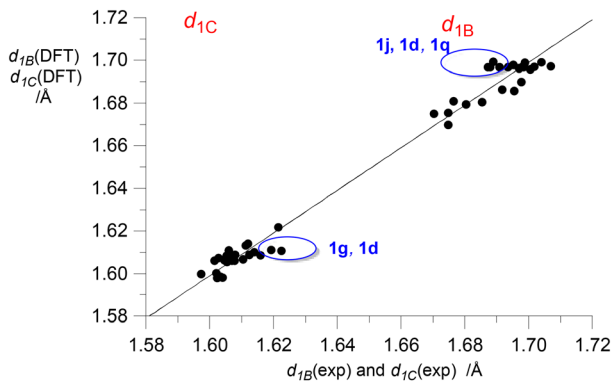

Fig. 10 A comparison of experimental and DFT-derived distances d_1 of the tetragonal pyramid in the {*closo*-1-CB_9} cluster in series **1** defined in Fig. 7. The line is the overall best fitting line from Fig. 8. The blue ovals indicate most outlying points.

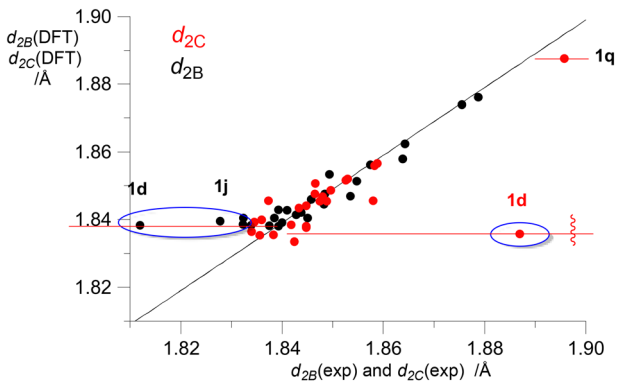

Fig. 11 A comparison of experimental and DFT-derived distances d_2 in the {*closo*-1-CB_9} cluster in series **1** defined in Fig. 7. The line is the overall best fitting line from Fig. 8. The blue ovals indicate the most outlying points.

 This journal is © The Royal Society of Chemistry 2023

Open Access Article. Published on 07 June 2023. Downloaded on 12/18/2025 6:25:32 PM. This article is licensed under a Creative Commons Attribution-NonCommercial 3.0 Unported Licence.

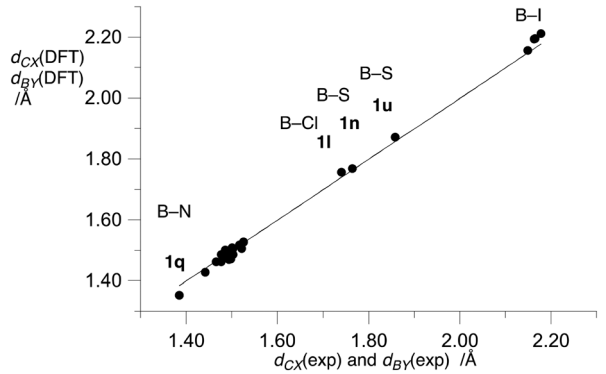

Fig. 12 Correlation of experimental and DFT-derived geometrical parameters d_{CX} and d_{CY} for the {*closo*-1-CB_9} cluster in series **1** as defined in Fig. 7. General best fitting line: d(DFT) = d(exp) − 0.001(1), r^2 = 0.996.

method in reproducing experimental structures. It revealed, however, significant problems with the experimental structure of **1d** (X═C_6H_4F) and, to a lesser extent, with **1q** (X═N_2^+, Y═I) and **1j** (X═CONHPr-*i*) consistent with poor structural data. On the other hand, this DFT method lacks high accuracy in dealing with the iodine atom.

The availability of the experimental and theoretical models in series **1** permits a brief comment on the conformational orientation of substituents attached to positions C(1) and B(10). Inspection of series **1** indicates five general types of architectures of substituents: four are shown in Fig. 13 (**A**–**D**) and the fifth type has the axial symmetry, such as N_2, I, Cl. Analysis of the DFT-optimized structures demonstrates strong preference for the staggered orientation of the apical substituents. In class **D**, the two Me groups in the NMe_3 substituent adopt a staggered conformation, while the third group eclipses the C(1)–B(2) bond, due to steric requirements of the C_3–symmetric substituent.

The orientation of substituents at the C(1) position in classes **A**, **B** and **D** is described by the torsion angle θ_X defined by X_β–X_α–C(1)–B(2) atoms, in which case θ_X = 0 corresponds to an ideal eclipsed conformation. Atoms α and β are successive atoms of the substituent. For the azo group in **A′** and substituents in **B′** the angle θ_X is defined as X_β–X_α–C(1)–B(6). The sulfonium substituent in class **C** assumes an ideal staggered conformation when the difference of two torsion angles measured for two substituents on the connecting atom (sulfur) θ_X–θ_X' = 0. Similarly, orientation of substituents at the B(10) position is defined by the analogous

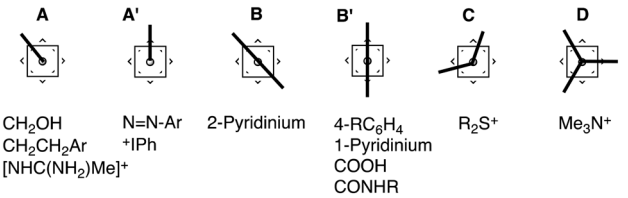

Fig. 13 Conformational ground states for four principal types (A–D) of substituents determined by DFT computational methods.

torsion angle θ_Y, *e.g.* for class **A′** and **B′**, θ_Y is defined by Y_β–Y_α–B(10)–B(5) atoms. Full details are listed in the ESI.†

Results of DFT calculations indicate that most substituents adopt either an ideal eclipsed (**A**, **B** and **D**) or staggered (**A′**, **B′** and **C**) orientation with respect to the {*closo*-1-CB_9} skeleton. The only exceptions are the C(1)–CH_2CH_2Ar (**1v** and **1u**) and NHC(NH_2)Me (**1y**) groups, which are about 10.5°, 12.1°, and 9.4°, respectively, away from the ideal eclipsed orientation. Also the C(1)–CONHPr-*i* group in **1j** is 12.1° away from the ideal staggered orientation. Interestingly, in contrast to 1-pyridinium in **1s** and **1x**, DFT predicts an eclipsed orientation for 2-pyridinium substituent in **1o** (class **B**), presumably due to electrostatic interactions between hydrogens atoms of significant protic and hydridic characters, $^+$N–H···H–B$^-$.

Analysis of experimental structures revealed that phenyl (**1c**, **1p**), 4-substituted phenyl (**1d**–**1g**, **1i**), 1-pyridinium (**1s**, **1x**) and carboxyl (**1r**–**1t**) substituents (class **B′**) generally conform to the staggered orientation relative to the {*closo*-1-CB_9} cage predicted by the DFT methods. The largest difference is observed for 1-pyridinium derivative **1x**, which deviates from the ideal orientation by 28.4°, and for the COOH group in **1s** and **1t** with an average deviation of about 14°. The CONHPr-*i* group in this class of substituents (**1j**) deviates by 25° from the orientation predicted by the DFT method (θ_X = 12.1°), and assumes a nearly eclipsed orientation.

The azo and IPh substituents in **1m** and **1u** (class **A′**) and also dimethylsulfonium substituent in **1n** (class **C**) little deviate from the ideal staggered orientation, by 4.8°, 14.6°, and 8.3°, respectively. In contrast, cyclic dialkylsulfonium group connected to the B(10) position in **1t** assumes orientation significantly is away from the ideal staggered: 30.3° off in molecule 1 and 65° in the second independent molecule. The NMe_3 in **1b** (class **D**) assumed an ideal eclipsed orientation, while 2-pyridinium in **1o** (class **B**) is away from DFT predicted position by 27°.

Finally, the CH_2CH_2Ar substituent in group **A** (**1u** and **1v**) is about 11° off the DFT-predicted pseudo eclipsed orientation ($\theta_X \approx 10.5°$), while the amidinium group in **1y** is closer to the staggered orientation (θ_Y = 32.9°) than to the predicted pseudo eclipsed form (θ_Y = 9.4°). The most significant discrepancy in the entire series is observed for the CH_2OH substituent in **1k**, for which the experimentally observed ideal staggered form in all four independent molecules in the solid is a rotational transition state in the DFT model, while the conformational ground state is the eclipsed form.

Substituent effect on the {*closo*-1-CB9} cage geometry

Analysis of structural data in series **1** indicates that the geometry of the {*closo*-1-CB_9} cage responses to the electronic nature of the apical substituents. The most convenient way to perform a quantitative analysis of such effects is by using

Open Access Article. Published on 07 June 2023. Downloaded on 12/18/2025 6:25:32 PM.
This article is licensed under a Creative Commons Attribution-NonCommercial 3.0 Unported Licence.

Hammett substituent parameters σ_p, which are well established for about half of the substituents in series **1**.[48] The σ_p parameters for 4-X–C_6H_4– substituents, where X = CN, COOH and N_2^+, were estimated from a correlation of the available[48] σ_p parameters for X and 4-XC_6H_4–, in which X = OMe, Me, Et, F, Cl, Br, I, NO_2.[47] Interestingly, the slope in this correlation is 0.32(2), which reflects the ability of two benzene rings (biphenyl) to transmit electronic effects. Hammett parameters σ_p for the PhI^+– (1.50), 1-$C_5H_5N^+$– (0.82), and $MeC(=NH_2)NH^+$– (0.48) groups were estimated previously with the accuracy of ±0.1 using a correlation of ^{1}H NMR chemical shifts of the C(1)–H proton in derivatives [*closo*-1-CB_9H_9–10-X]$^-$ and known σ_p values.[33,47] A substituent parameter for the 2-$C_5H_5N^+$ group in **1o** remains unavailable. The analysis also excludes **1d**, which shows significant problems with conforming to structural trends established for the entire series.

Available data allow for a separate analysis of the substituent effect at the C(1) (12 derivatives **1b**–**1n**) or at both apical positions (10 derivatives **1p**–**1y**) on the {*closo*-1-CB_9} cage geometry. Analysis of the first group of derivatives demonstrates essentially no effect on the heights of the square pyramids, h_C and h_B. Both values are constant within the experimental error in the series (average 0.941(9) Å and 1.092(6) Å, respectively), despite a significant range of σ_p values (0–0.90) of the C(1) substituents (Fig. 14). Other distances defined in Fig. 7, *d* and *s*, are nearly constant in the series of C(1) substituted derivatives.[47] The largest, although still marginal impact of the C(1) substituent is observed for the d_{2C} parameter (the B(2)–B(3) distance), which increases at a rate of 0.020(6) Å/σ_p.

A similar analysis for the second group of derivatives, those containing substituent at the B(10) position showed a much stronger substituent effect on {*closo*-1-CB_9} cage geometry. Since in most derivatives **1p**–**1y** both apical positions are substituted, for the purpose of the analysis a sum of two Hammett constants was used. This approach was successful in analysis of [*closo*-$B_{10}H_{10}$]$^{2-}$ dianion derivatives.[37] Results demonstrate that the heights of the two square pyramids response to the apical substituents; both parameters decrease as the electron withdrawing character of the substituents increases. This response is over twice greater for the B(10) pyramid (h_B) than for the C(1) pyramid (h_C, Fig. 15). Consequently, the overall length of the {*closo*-1-CB_9} cage, *l*, decreases at a rate −0.044 Å/$\sum\sigma_p$ with increasing electron demand of the substituents, despite the fact that the distance between the equatorial planes is essentially unaffected (Fig. 16).

The apical substituents also visibly affect distances d_C and d_B, particularly the equatorial B–B bond lengths (d_{2C} and d_{2B}), which expand with increasing value of the σ_p parameter at a rate of about 0.012 Å/$\sum\sigma_p$ (Fig. 17). Out of the two d_1 parameters, only d_{1B} (the B(10)–B distances) is affected by the apical substitution and it decreases (slope −0.009(5) Å/$\sum\sigma_p$), while d_{1C} is constant within the experimental error (avrg 1.608(6) Å).

Analysis for the entire set of derivatives **1** revealed similar dependence of key structural parameters, *h*, *d* and *s* on the sum of the Hammett constants, as observed for the series **1p**–**1y**.

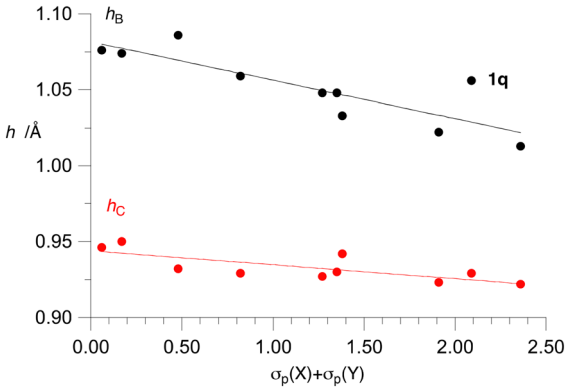

Fig. 15 A plot of parameters h_C and h_B *vs.* sum of σ_p(X) and σ_p(Y) values in series **1p**–**1y**. Best fitting functions: h_C = 0.944(4) − 0.009(3) × [σ_p(X) + σ_p(Y)], r^2 = 0.58; h_B = 1.082(8) − 0.025(6) × [σ_p(X) + σ_p(Y)], r^2 = 0.72.

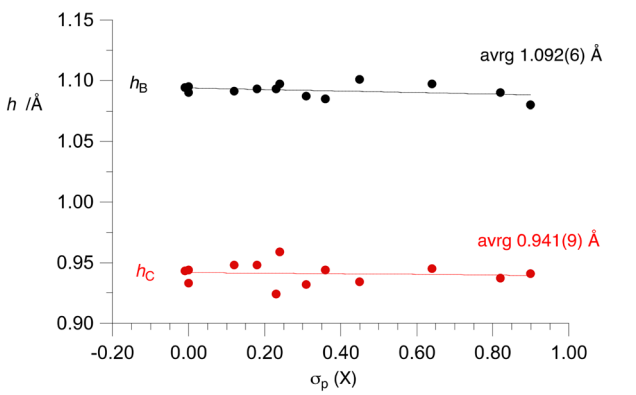

Fig. 14 A plot of parameters h_C and h_B *vs.* σ_p(X) values for substituents at C(1) in series **1a**–**1n** (**1d** is excluded).

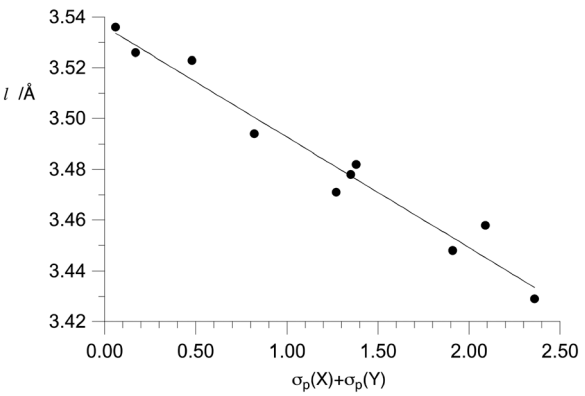

Fig. 16 A plot of the total length of the {*closo*-1-CB_9} cluster *vs.* sum of σ_p(X) and σ_p(Y) values in series **1p**–**1y**. Best fitting function: *l* = 3.536(4) − 0.044(3) × [σ_p(X) + σ_p(Y)], r^2 = 0.96.

This journal is © The Royal Society of Chemistry 2023

Open Access Article. Published on 07 June 2023. Downloaded on 12/18/2025 6:25:32 PM.
This article is licensed under a Creative Commons Attribution-NonCommercial 3.0 Unported Licence.

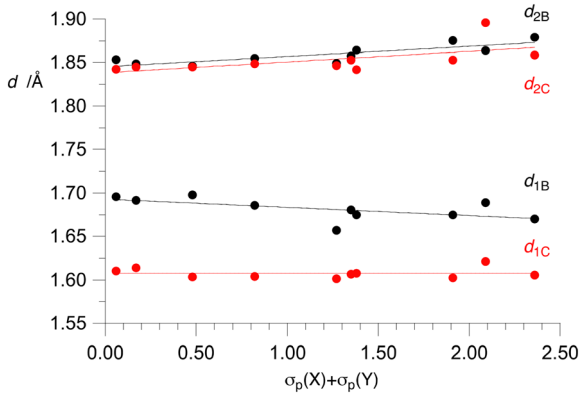

Fig. 17 A plot of parameters d_C and d_B *vs.* sum of σ_p(X) and σ_p(Y) values in series **1p**–**1y**. Best fitting functions: d_{2C} = 1.838(8) + 0.012(6) × [σ_p(X) + σ_p(Y)], r^2 = 0.38; d_{2B} = 1.845(4) + 0.012(6) × [σ_p(X) + σ_p(Y)], r^2 = 0.69.

Conclusions

Recent advances in the chemistry of the [*closo*-1-CB_9H_{10}]$^-$ anion (**1a**) opened up a facile access to the parent anion itself and to its B(10) derivatives, which resulted in an increasing number of experimental structures. Analysis of a set of 24 structures demonstrates that the experimental geometrical parameters of the {*closo*-1-CB_9} cage are well reproduced by the B3LYP/Def2TZVP method in PhCl dielectric medium, giving an excellent overall correlation. The most common outliers in the analysis are **1d** and **1q**. The problem with fitting the former is related to poor experimental data, while deviations for **1q** data points are possibly due to inaccurate DFT modeling of the iodine atom. Detailed analysis demonstrated good correlations for parameters h_B, h_C, and l, moderate quality for parameters d_{1C}, d_{2C}, d_{2B}, and d_{1B}, while the lowest agreement between theoretical and experimental values were observed for parameter s. On the other hand, the experimental exocyclic bonds (d_{CX} and d_{BY}) were well reproduced with the DFT method.

Structural analysis of series **1** revealed that substitution of the C(1) position with groups characterized by the Hammett σ_p parameter in a rage of 0.0–0.90 (derivatives **1b**–**1n**) has a negligible effect on the {*closo*-1-CB_9} cage geometry. In contrast, the B(10) substituents in series **1p**–**1y** affect the cage geometry, and the effect is generally stronger for the square pyramid containing the B(10) atom than on the C(1) pyramid. Thus, the heights of the pyramids and consequently the overall length of the {*closo*-1-CB_9} cage contracts with increasing electron-withdrawing character of the substituents. This is consistent with trends found in derivatives of the [*closo*-$B_{10}H_{10}$]$^{2-}$ dianion.[35–37] At the same time, bases of both square pyramids expand (cage widening), while the edge marginally contracts only for the B(10) pyramid.

Overall, the presented analysis suggests that the B3LYP/Def2TZVP method well reproduces experimental structures, while the uncovered trends in substituent effects can effectively be used as guides in structural analysis of [*closo*-1-CB_9H_{10}]$^-$ anion derivatives.

Author contributions

Conceptualization, data analysis, visualization, writing, and editing – P. Kaszyński and A. Pietrzak; XRD measurements – M. J. Carr.

Conflicts of interest

There are no conflicts to declare.

Acknowledgements

This project was supported by the National Science Foundation (DMR-1611250). Single crystal X-ray measurements were supported with the UK EPSRC for instrumental grants M83360 and R61949. A. P. thanks the Faculty of Chemistry, Lódź University of Technology for Young Scientists' Fund (grant W-3D/FMN/1G/2022). M. J. C. thanks Andy Franken and John D. Kennedy for help with acquiring the XRD data.

References

1 R. N. Grimes, *Carboranes*, Academic Press, Boston, 2nd edn, 2011.
2 S. P. Fisher, A. W. Tomich, S. O. Lovera, J. F. Kleinsasser, J. Guo, M. J. Asay, H. M. Nelson and V. Lavallo, *Chem. Rev.*, 2019, **119**, 8262–8290.
3 B. Ringstrand and P. Kaszynski, *Acc. Chem. Res.*, 2013, **46**, 214–225and references therein.
4 Y. Zhu and N. S. Hosmane, *Eur. J. Inorg. Chem.*, 2017, 4369–4377.
5 J. Dymon, R. Wibby, J. Kleingardner, J. M. Tanski, I. A. Guzei, J. D. Holbrey and A. S. Larsen, *Dalton Trans.*, 2008, 2999–3006.
6 A. S. Larsen, J. D. Holbrey, F. S. Tham and C. A. Reed, *J. Am. Chem. Soc.*, 2000, **122**, 7264–7272.
7 J. Pecyna, A. Sivaramamoorthy, A. Jankowiak and P. Kaszynski, *Liq. Cryst.*, 2012, **39**, 965–971.
8 B. Ringstrand, A. Jankowiak, L. E. Johnson, P. Kaszynski, D. Pociecha and E. Górecka, *J. Mater. Chem.*, 2012, **22**, 4874–4880.
9 B. Ringstrand, H. Monobe and P. Kaszynski, *J. Mater. Chem.*, 2009, **19**, 4805–4812.
10 R. Jay, A. W. Tomich, J. Zhang, Y. Zhao, A. De Gorostiza, V. Lavallo and J. Guo, *ACS Appl. Mater. Interfaces*, 2019, **11**, 11414–11420.
11 S. G. McArthur, R. Jay, L. Geng, J. Guo and V. Lavallo, *Chem. Commun.*, 2017, **53**, 4453–4456.
12 J. Guschlbauer, L. Niedzicki, L. Jacob, E. Rzeszotarska, D. Pociecha and P. Kaszyński, *J. Mol. Liq.*, 2023, **377**, 121525.
13 B. Ringstrand and P. Kaszynski, *J. Mater. Chem.*, 2011, **21**, 90–95.

Open Access Article. Published on 07 June 2023. Downloaded on 12/18/2025 6:25:32 PM.
This article is licensed under a Creative Commons Attribution-NonCommercial 3.0 Unported Licence.

14 R. Jakubowski, J. Pecyna, M. O. Ali, A. Pietrzak, A. C. Friedli and P. Kaszyński, *Dalton Trans.*, 2021, **50**, 3671–3681.
15 J. Pecyna, R. Żurawiński, P. Kaszyński, D. Pociecha, P. Zagórski and S. Pakhomov, *Eur. J. Inorg. Chem.*, 2016, 2923–2931.
16 P. Kaszyński, in *Handbook of Boron Science*, ed. N. S. Hosmane and R. Eagling, World Scientific, London, 2018, vol. 3, pp. 57–114.
17 B. Brellochs, in *Contemporary Boron Chemistry*, ed. M. G. Davidson, A. K. Hughes, T. B. Marder and K. Wade, Royal Society of Chemistry, Cambridge, England, 2000, pp. 212–214.
18 I. B. Sivaev, Z. A. Starikova, P. V. Petrovskii, V. I. Bregadze and S. Sjöberg, *J. Organomet. Chem.*, 2005, **690**, 2790–2795.
19 K. Nestor, B. Štibr, J. D. Kennedy, M. Thornton-Pett and T. Jelinek, *Collect. Czech. Chem. Commun.*, 1992, **57**, 1262–1268.
20 B. Štibr, J. Plešek, T. Jelinek, J. D. Kennedy and M. Thornton-Pett, *J. Chem. Soc., Dalton Trans.*, 1997, 4231–4236.
21 T. Jelinek, C. A. Kilner, M. Thornton-Pett and J. D. Kennedy, *Chem. Commun.*, 2001, 1790–1791.
22 S. L. Renard, A. Franken, C. A. Kilner, J. D. Kennedy and M. A. Halcrow, *New J. Chem.*, 2002, **26**, 1634–1637.
23 V. I. Bragin, A. A. Korlyukov, P. V. Petrovskii, I. B. Sivaev and V. I. Bregadze, *J. Fluorine Chem.*, 2012, **142**, 14–18.
24 A. Franken, M. J. Carr, W. Clegg, C. A. Kilner and J. D. Kennedy, *Dalton Trans.*, 2004, 3552–3561.
25 A. V. Shmalko, K. Y. Suponitsky, I. B. Sivaev and V. I. Bregadze, *Russ. Chem. Bull.*, 2022, **71**, 399–403.
26 A. Franken, C. A. Kilner and J. D. Kennedy, *Inorg. Chem. Commun.*, 2003, **6**, 1104.
27 X. Liang, Y. Shen, K. Zhang, J. Liu and S. Duttwyler, *Chem. Commun.*, 2018, **54**, 12451–12454.
28 B. Ringstrand, P. Kaszynski and A. Franken, *Inorg. Chem.*, 2009, **48**, 7313–7329.
29 A. Franken, C. A. Kilner, M. Thornton-Pett and J. D. Kennedy, *Collect. Czech. Chem. Commun.*, 2002, **67**, 869–912.
30 B. Ringstrand, A. Balinski, A. Franken and P. Kaszynski, *Inorg. Chem.*, 2005, **44**, 9561–9566.
31 B. Ringstrand, P. Kaszynski, V. G. Young Jr. and Z. Janoušek, *Inorg. Chem.*, 2010, **49**, 1166–1179.
32 P. Kaszyński and B. Ringstrand, *Angew. Chem., Int. Ed.*, 2015, **54**, 6576–6581.
33 R. Żurawiński, R. Jakubowski, S. Domagała, P. Kaszyński and K. Woźniak, *Inorg. Chem.*, 2018, **57**, 10442–10456.
34 R. Jakubowski, A. Pietrzak, A. C. Friedli and P. Kaszyński, *Chem. – Eur. J.*, 2020, **26**, 17481–17494.
35 L. Jacob, E. Rzeszotarska, A. Pietrzak, V. G. Young Jr. and P. Kaszyński, *Eur. J. Inorg. Chem.*, 2020, 3083–3093.
36 S. Kapusciński, M. B. Abdulmojeed, T. E. Schafer, A. Pietrzak, O. Hietsoi, A. C. Friedli and P. Kaszyński, *Inorg. Chem. Front.*, 2021, **8**, 1066–1082.
37 L. Jacob, E. Rzeszotarska, M. Koyioni, R. Jakubowski, D. Pociecha and A. Pietrzak, *Chem. Mater.*, 2022, **34**, 6476–6491.
38 Z. Otwinowski and W. Minor, in *Methods in Enzymology*, ed. C. W. Carter and R. M. Sweet, Academic Press, 1997, vol. 276, pp. 307–326.
39 *COLLECT, Data Collection Strategy Program*, Nonius, 1999.
40 G. M. Sheldrick, *SHELXS-97, Program for crystal structure solution*, University of Göttingen, 1997.
41 G. M. Sheldrick, *SHELXL-97, Program for crystal structure refinement*, University of Göttingen, 1997.
42 A. D. Becke, *J. Chem. Phys.*, 1993, **98**, 5648–5652.
43 C. Lee, W. Yang and R. G. Parr, *Phys. Rev. B*, 1988, **37**, 785–789.
44 F. Weigend, *Phys. Chem. Chem. Phys.*, 2006, **8**, 1057–1065.
45 F. Weigend and R. Ahlrichs, *Phys. Chem. Chem. Phys.*, 2005, **7**, 3297–3305.
46 M. Cossi, G. Scalmani, N. Rega and V. Barone, *J. Chem. Phys.*, 2002, **117**, 43–54 and references therein.
47 For details see the ESI†.
48 C. Hansch, A. Leo and R. W. Taft, *Chem. Rev.*, 1991, **91**, 165–195.

 This journal is © The Royal Society of Chemistry 2023